Ribosomal Protein SA (RPSA) is required for localized translation and sarcomere maintenance

Omer Sadeh[1,2], Rami Haddad[1,2], Tamar Ziv[3], Lilac Haimovich-Caspi[2], Ariel Shemesh[4], Izhak Kehat*[2,5]

[1]These authors contributed equally

[2]The Rappaport Institute and the Bruce Rappaport Faculty of Medicine, Technion – Israel Institute of Technology, 1 Efron Street, P.O. Box 9697 Haifa 3109601, Israel.

[3]Smoler Proteomics Center, Lorry I. Lokey Interdisciplinary Center for Life Sciences and Engineering, Technion-Israel Institute of Technology

[4]Biomedical Core Facility at the Faculty of Medicine, Technion-Israel Institute of Technology

[5]Lead contact

*Correspondence: ikehat@technion.ac.il

Keywords:

Ribosome

Localized translation

Sarcomere

Z-line

Summary

Cardiomyocyte sarcomeres contain localized ribosomes, but the factors responsible for their localization and the significance of localized translation are unknown. Using proximity labeling, we identified Ribosomal Protein SA (RPSA) as a Z-line protein. In cultured cardiomyocytes, the loss of RPSA led to impaired local protein translation and reduced sarcomere integrity. By employing CAS9 expressing mice along with adeno-associated viruses expressing CRE recombinase and single-guide RNAs targeting *Rpsa*, we knocked out RPSA in vivo and observed mis-localization of ribosomes and diminished local translation. These genetic mosaic mice with RPSA knockout in a subset of cardiomyocytes developed dilated cardiomyopathy, featuring atrophy of RPSA-deficient cardiomyocytes, compensatory hypertrophy of unaffected cardiomyocytes, left ventricular dilation, and impaired contractile function. We demonstrate that RPSA C-terminal domain is sufficient for localization to the Z-lines. These findings highlight RPSA as a ribosomal factor responsible for ribosome localization to the Z-line, facilitating local translation and sarcomere maintenance.

Introduction

Local translation has several benefits over diffuse or unlocalized protein production. Importantly, it allows protein synthesis closer to the site of action, is more economic, may prevents protein aggregation, and can facilitate processes such as co-translational assembly.[1] Local translation requires the presence of the mRNA, the ribosome, as well as additional translation factors and co-factors. While the localization of mRNAs and the RNA-binding protein involved, particularly in neurons, are well studied[2], the factors involved in the localization of cytoplasmic ribosomes are less clear.

The sarcomere is the basic contractile element of cardiomyocytes. Because its protein constituents have a limited half-life, this complex must be continuously maintained.[3] failure in sarcomeric proteostasis may lead to heart failure because failing human hearts have reduced sarcomere and sarcomeric protein content.[4–6] We previously showed that ribosomes are localized on both sides of the Z-line of the sarcomere, and that proteins are translated there, leading us to propose that sarcomeres are maintained by the localized translation of proteins within them.[7] We have also demonstrated that the microtubule cytoskeleton and kinesin are essential for localized translation in the heart.[7,8]. Similar observations were made for skeletal muscles.[9] Yet, the importance of localized translation for sarcomere maintenance has not been demonstrated, and the ribosomal factors required for localization are unknown.

Here we used proximity labeling to elucidate the proteomic composition of sarcomeric Z-lines in an unbiased manner and identified Ribosomal Protein SA (RPSA), a protein with reported ribosome and laminin receptor functions. We show that loss of RPSA in cultured cardiomyocytes results in the loss of local protein translation and in reduced sarcomere integrity. Using conditional and unconditional CAS9 expression mice and adeno-associated viruses (AAVs) expressing CRE recombinase in cardiomyocytes with single-guide RNAs (sgRNAs) targeting *Rpsa* we knocked out RPSA in cardiomyocytes in vivo and show that the loss of RPSA results in mis-localization of ribosomes and reduced local protein translation. These genetic mosaic mice, where only a portion of cardiomyocytes are transduced and have RPSA knockout, develop a dilated cardiomyopathy with atrophy of RPSA knockout cardiomyocytes, compensatory hypertrophy of untransduced cardiomyocytes, left ventricular dilation and reduced contractile function. RPSA is known to directly bind the microtubular system and we show its C-terminal domain is sufficient for localization to Z-lines. These data show RPSA, the first ribosomal factor responsible for localizing cytoplasmic ribosomes identified, is required for localization of ribosomes to the Z-line, for the local translation there, and for the maintenance of the sarcomere.

Results

Proximity-dependent labeling identifies components of translational machinery at sarcomeric Z-lines

To investigate the proteomic composition of sarcomeric Z-lines and identify the factors involved in localized translation, we employed the BioID2 proximity labeling assay using Cypher (LDB3), a known Z-line protein, as bait. For this purpose, we generated a fusion construct between Cypher and the promiscuous biotin ligase BioID2. We then transduced neonatal rat ventricular cardiomyocytes (NRVMs) with an adenoviral vector encoding for Cypher-BioID2 or control virus expressing BioID2 alone. To confirm the correct subcellular localization of our fusion construct we first performed immunofluorescence staining that demonstrated that Cypher-BioID2 fusion construct closely matched the known localization pattern of endogenous Cypher at the sarcomeric Z-lines, whereas BioID2-alone displayed a more diffuse cytoplasmic staining (Figure 1A). We then used three independent samples for each group, each containing 12 million cardiomyocytes, and purified biotinylated proteins using streptavidin-coated magnetic beads after 18 hours of incubation with biotin. Western blot analysis of the extracted cardiac proteins, using a streptavidin probe confirmed the successful biotinylation of proteins and showed distinct

sets of labeled proteins in the Cypher-BioID2 sample compared to the BioID2-alone control samples (Figure 1B).

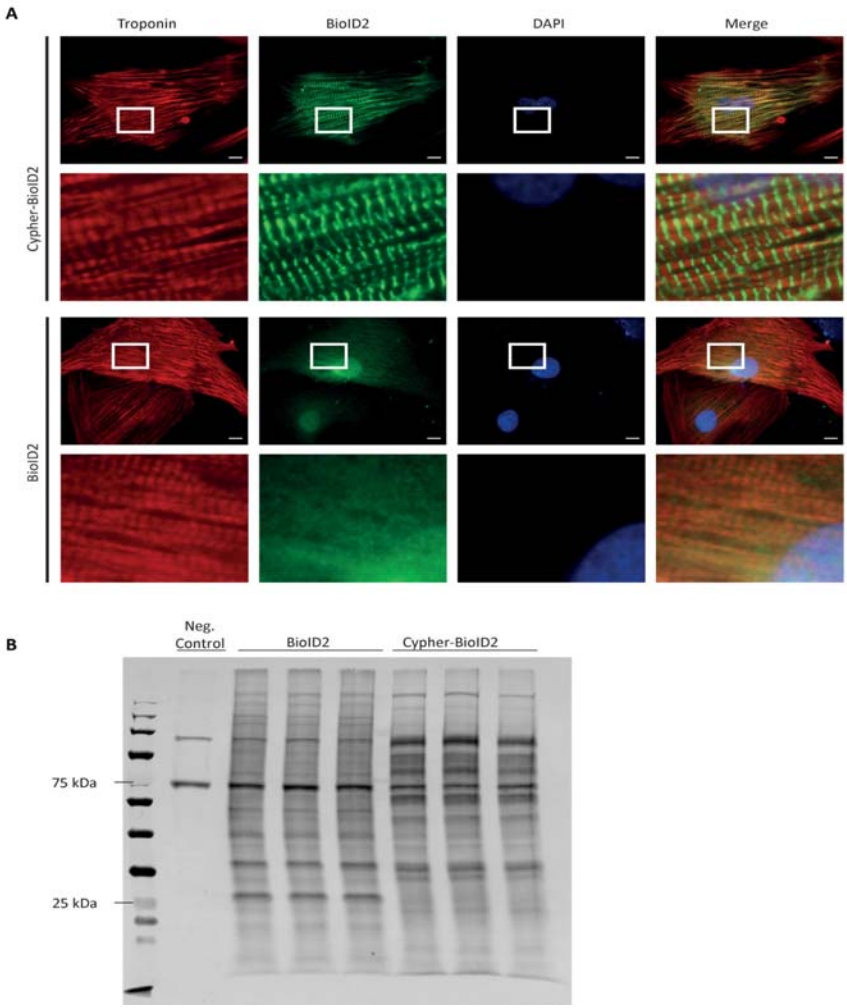

Figure 1. Cypher-BioID2 is localized to the Z-lines and biotinylate specific proteins.

(A) Representative immunofluorescence images of NRVMs transduced with adenoviruses encoding for either Cypher-BioID2 (bait construct) or BioID2 (control construct) with inset showing Z-line localization of Cypher-BioID2 and a diffuse cytoplasmic localization for BioID2 alone. Samples were immunostained for cardiac troponin (red), BioID (green) and DAPI (blue). Scale bar = 10 µm.

(B) Western blot analysis of biotinylated proteins using IRDye800-Streptavidin showing different biotinylated patterns for cardiomyocytes transduced with BioID2 or Cypher-BioID2 and minimal biotinylation of the untransduced negative control sample. Each lane was loaded with 100 µg of protein lysate.

Pulled down proteins were trypsin digested on beads and subjected to mass spectrometry analysis. The proteomic analysis identified 135 proteins significantly enriched in the Cypher-BioID2 sample compared to the BioID2-alone control using a cutoff of more than 2-fold enrichment (log2 FC≥1) and t test p value <0.05 (Figure 2A, Table 1). As expected, LDB3 (Cypher), that served as the bait, was the most abundant and most significantly enriched protein in the bait group. Proteins known to be localized to the Z-line, such as α-Actinin (ACTN2) and titin (TTN), were also significantly enriched in the bait group. On the other hand, highly expressed proteins known to be localized to the M-line such as MYOM1 (Myomesin1) or OBSCN (Obscurin) were significantly more abundant in the control group, demonstrating we have specifically enriched for a Z-line nanodomain. Additional proteins significantly enriched in the bait group included RPSA (Ribosomal Protein SA), and RPL38 (Ribosomal Protein L38).

To gain insight into the protein groups associated with the Cypher-BioID2 significantly enriched proteins (fold change ≥ 2 and p value < 0.05), we performed an enrichment analysis using gene ontology (GO) terms. The analysis indicated that the Cypher-BioID2 associated proteins were significantly enriched in several terms, including ribosome and sarcomere Z-line, further confirming our previous observation that the Z line region contains a protein translation nanodomain (Figure 2B). There is an inherent overlap among GO terms, as a given protein can be associated with multiple terms. We therefore also employed an unsupervised clustering approach with the aim of identifying distinct clusters of enriched GO terms. This analysis revealed two major clusters of protein functions. The first cluster consisted of pathways related to translational machinery, such as ribosomal proteins and ribonucleoprotein complexes. The second cluster included pathways involved in cytoskeletal elements, particularly those associated with sarcomeric structures (Figure 2C). This analysis showsindicates that the two main functions of the Z line nanodomain are contractile-cytoskeletal function and protein translation. All Cypher-BioID2 enriched proteins are also shown in a STRING analysis (Figure S1).

Of the identified proteins we decided to concentrate on Ribosomal Protein SA (RPSA). RPSA is considered a ribosomal protein which has acquired the function of laminin receptor during evolution. Although its function in the heart is not known, it was reported to bind both ribosomes and the microtubular system.[10] We also studied Ribosomal Protein L38 (RPL38), a known component of the 60S subunit of the ribosome. We performed immunofluorescence staining of RPSA in adult rat cardiomyocytes showing RPSA was aligned on both sides of the α-actinin

containing Z lines (Figure 2D). This result further validates our proximity labeling approach and confirms that RPSA is localized to sarcomeric Z lines.

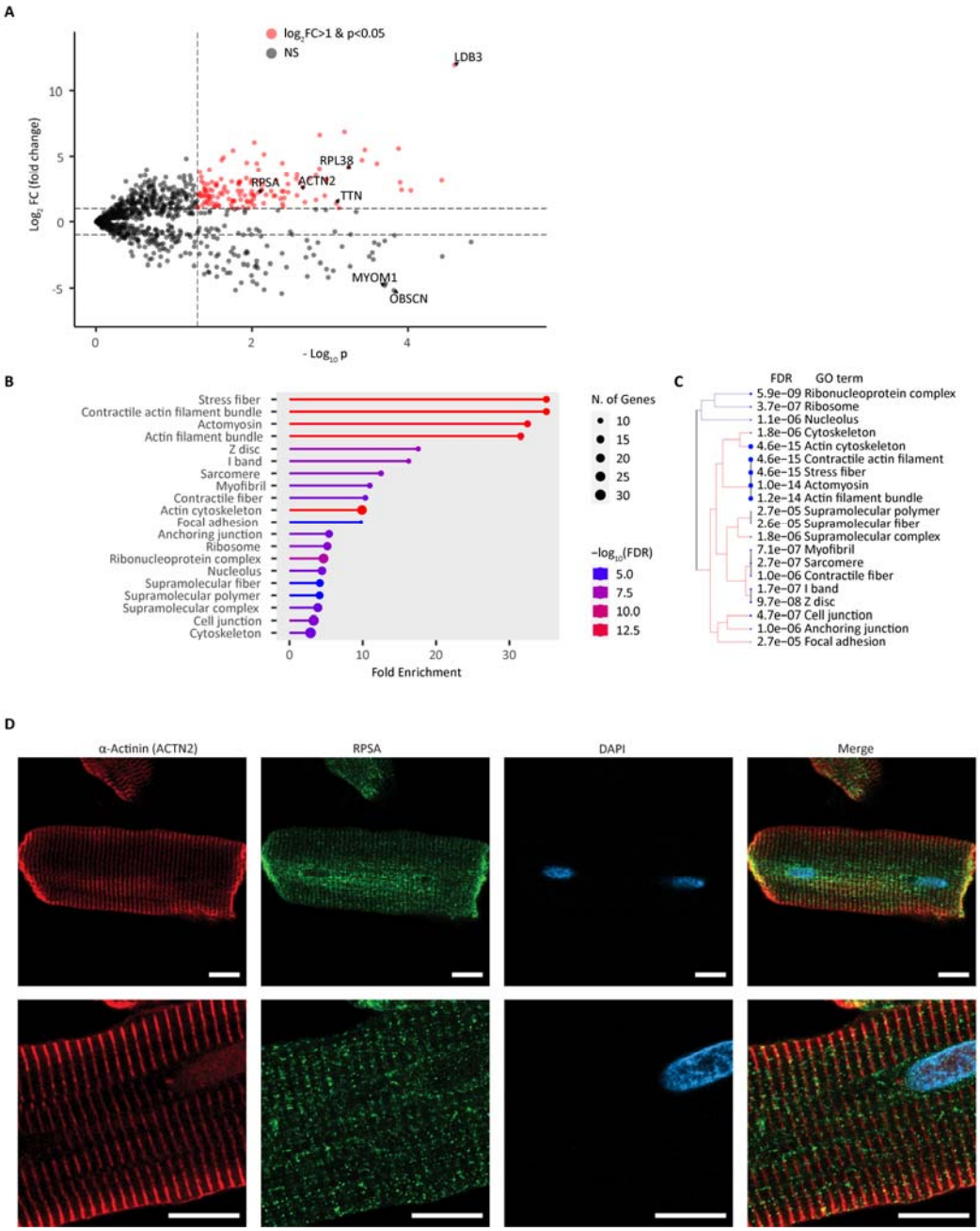

Figure 2. Proximity- labeling with Cypher-BioID2 identifies Z-line proteins and components of the translational machinery

(A) Volcano plot of proteins identified by mass spectrometry showing the $\log_2$ fold change in protein abundance with Cypher-BioID2 vs. BioID2 alone and the t test $-\log_{10}$ (p value) of the

difference significance. Dashed horizontal bars show the >2 or <2 cutoffs for fold change and the vertical dashed bar shows the p<0.05 cutoff for significance. Proteins highlighted in red are those with a fold change ≥ 2 and p value < 0.05 that were used for further pathway enrichment analysis. Other proteins were denoted as non-significant (NS) and are shown in grey. Several significantly identified proteins are highlighted.
(B) Pathway enrichment analysis of BioID2 significantly enriched proteins (fold change ≥ 2 and p value < 0.05) showing fold enrichment of GO terms associated with cytoskeletal elements of the sarcomere and with ribosomes and protein translation. The number of proteins identified for each term is shown as a circle and the $-\log_{10}$ of the false discovery rate (FDR) is color coded.
(C) Unsupervised clustering of enriched GO terms showing identified proteins were predominantly associated with two main groups – Cytoskeletal sarcomere proteins or ribosomal componenets. The enrichment FDR of specific GO terms is shown.
(D) Representative immunofluorescence images of isolated adult rat ventricular cardiomyocytes stained for α-actinin (red), RPSA (green) and DAPI (blue) showing localization of endogenous RPSA to both sides of the Z-line identified with α-Actinin. Scale bar = 10 µm.

Loss of RPSA disrupts localized translation and sarcomeric integrity in cultured cardiomyocytes

The localization of RPSA on both sides of the Z-line suggested that in cardiomyocytes this protein has a ribosomal rather than a laminin receptor function. We therefore asked if RPSA is required for localized protein translation in the sarcomere and for sarcomere maintenance. We used siRNA to knockdown RPSA in NRVMs, or knocked down RPL38, a known ribosomal protein as a control. The efficacy of the *Rpsa* knockdown was validated by quantitative PCR (RT-qPCR), which demonstrated an ~85% reduction in *Rpsa* and ~82% reduction in *Rpl38* mRNA levels compared to the non-targeting negative control siRNA group (Figure 3A). A reduction in RPSA protein levels was also confirmed using Western blotting (Figure 3B).

To assess the effect of *Rpsa* or *Rpl38* knockdown on localized protein translation, the control and knockdown cells were incubated with OPP, a puromycin analogue that labels newly translated proteins, for 60 minutes. Cardiomyocytes were fixed, OPP incorporated nascent peptides were labeled using Alexa Fluor 488 by a Click reaction and immunostained with antibodies against sarcomeric ACTN2 to examine the sarcomeric structure. This analysis revealed a major disruption in localized protein synthesis with knockdown of *Rpsa*, but not with

knockdown of *Rpl38* or control siRNA knockdown (Figure 3C). The sarcomere structure on the other hand appeared largely intact.

To quantify these changes, we used an automated image processing approach inspired by the Sarcomere Texture Analysis (SOTA) method.[11] These custom tools segment cells from multi-channel immunofluorescence images and employ algorithms to quantify two aspects of the sarcomeric structure, namely homogeneity and co-localization of different markers. Homogeneity score is a measure of the uniformity of signal distribution in the image, with a higher score indicating a more diffuse signal distribution, and a lower score indicating a more localized distribution (Figure 3D). This unbiased automated analysis showed that the knockdown of RPSA resulted in a statistically significant increase in homogeneity in the OPP signals (Figure 3E), indicating a loss of localized protein translation with a shift toward more diffuse translation. While our visual analysis did not reveal a major disruption in the sarcomere organization, our automated analysis of the α-actinin (ACTN2) staining demonstrated an impairment (Figure 3F). The automated analysis also revealed a significant decrease in the co-localization between the ACTN2 and OPP signals after *Rpsa* knockdown (Figure 3G), indicating a much greater loss of sarcomeric localized translation relative to the changes in sarcomeric structure. In contrast with these findings the loss of RPL38 did not affect the localization of translation or the integrity of the sarcomere. Together these data indicate that the loss of RPSA results in the loss of sarcomeric Z-line protein translation and a likely secondary loss of sarcomere structure in cardiomyocytes.

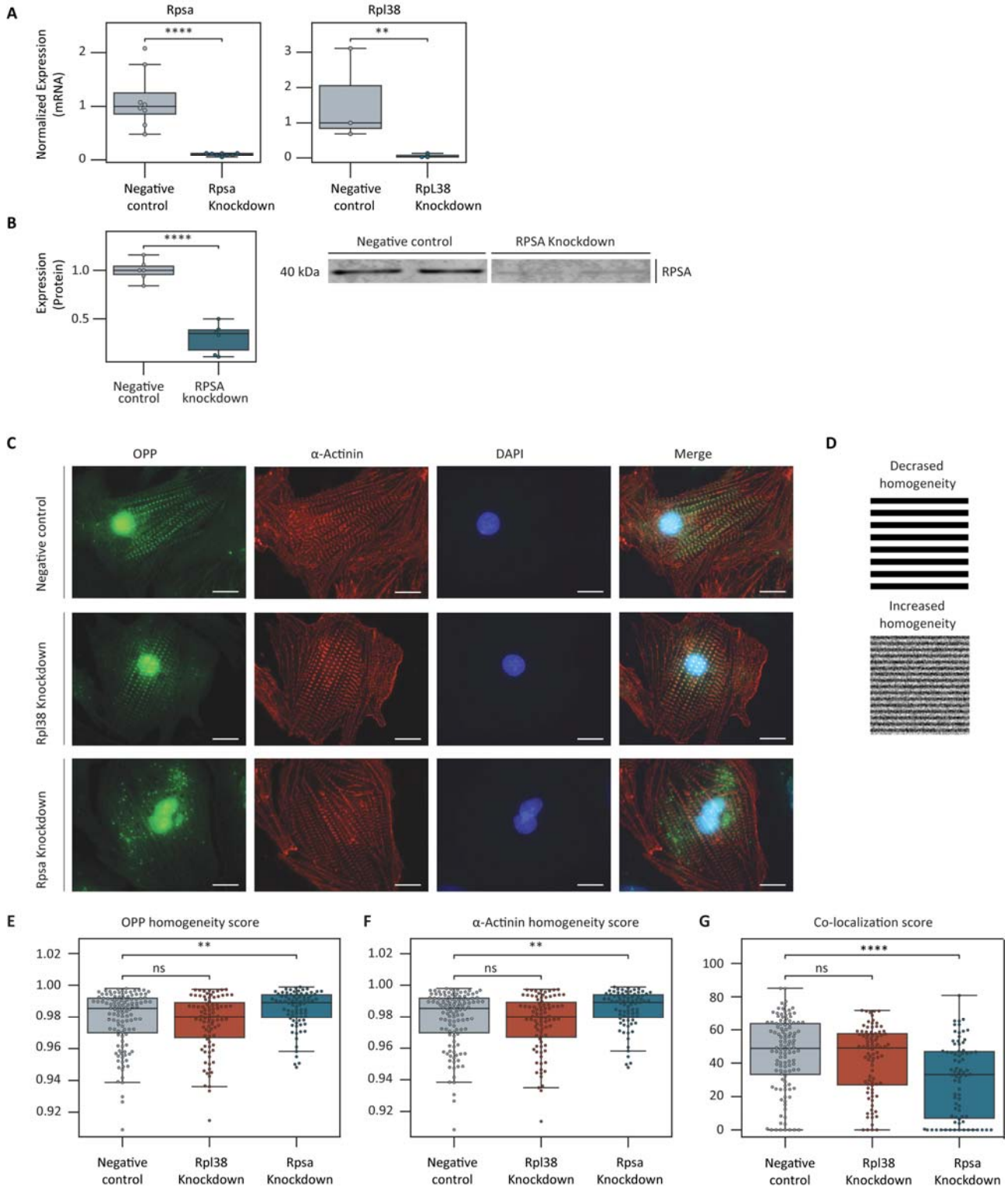
A
Rpsa
Rpl38
Normalized Expression (mRNA)
****
**
Negative control
Rpsa Knockdown
RpL38 Knockdown
B
Expression (Protein)
Negative control
RPSA knockdown
Negative control
RPSA Knockdown
40 kDa
RPSA
C
OPP
α-Actinin
DAPI
Merge
Negative control
Rpl38 Knockdown
Rpsa Knockdown
D
Decrased homogeneity
Increased homogeneity
E
OPP homogeneity score
ns
F
α-Actinin homogeneity score
G
Co-localization score

Figure 3. Knockdown of RPSA disrupts localized translation in cultured cardiomyocytes
(A) Gene expression analysis with RT-qPCR of *Rpsa* (left) and *Rpl38* (right) shows ~85% and ~82% reduction in expression levels following siRNA-mediated knockdown respectively compared with control siRNA. Expression was normalized to *Gapdh*. N = 3-8 biological samples per experimental group pooled from 3 independent experiments. Unpaired t-test p value annotation: ns ($p > 0.05$), * ($p \leq 0.05$), ** ($p \leq 0.01$), *** ($p \leq 0.001$), **** ($p \leq 0.0001$).
(B) Representative image of western blot analysis (right) with densitometric analysis (left) of RPSA protein expression shows a~70% reduction in RPSA protein levels compared to control following siRNA-mediated knockdown. N = 6 biological samples per experimental group from 3 independent experiments. Unpaired t-test p value annotation: **** ($p \leq 0.0001$).
(C) NRVMs were incubated with o-propargyl-puromycin (OPP) to label nascent proteins 48 hours after treatment with negative control (top), *Rpl38* (middle), or *Rpsa* (bottom) siRNAs. Representative images of staining for OPP-labeled nascent proteins (green), α-actinin (red) and DAPI (blue) show disruption of localized protein synthesis following RPSA knockdown but not following RPL38 knockdown or under control conditions. Scale bar = 10 µm.
(D) Cartoon to illustrate a structure with decreased homogeneity (top) and a structure with increased homogeneity (bottom).
(E-F) Homogeneity scores for translation from the OPP signal (E) and for the sarcomeric structure from the α-Actinin signal (F), showing increased homogeneity implying decreased localization following RPSA knockdown but not following RPL38 knockdown or using control siRNAs. N = 119-172 cells per group pooled from 4 independent experiments. p value annotation: ns ($p > 0.05$), * ($p \leq 0.05$), ** ($p \leq 0.01$), *** ($p \leq 0.001$), **** ($p \leq 0.0001$).
(G) Co-localization analysis between the OPP and the α-Actinin signal showing significantly decreased co-localization between translation and the Z-line after knockdown of RPSA. N = 119-172 cells per group pooled from 4 independent experiments. p value annotation: ns ($p > 0.05$), * ($p \leq 0.05$), ** ($p \leq 0.01$), *** ($p \leq 0.001$), **** ($p \leq 0.0001$).

Loss of RPSA results in cardiac disfunction in-vivo

We next wanted to study the consequences of RPSA loss in cardiomyocytes in vivo. We first used Rosa26-Lox-stop-Lox-Cas9 knockin mice, which have a floxed-STOP cassette preventing the expression of the downstream CRISPR associated protein 9 (CAS9) endonuclease knocked in the Rosa26 locus. These mice were crossed in the Jackson Laboratory to a β-actin driven

CRE recombinase strain, resulting in the ubiquitous and strong expression of CAS9 under the control of the CAG promoter in multiple tissues, including the heart. Studies in the Jackson Laboratory showed that constitutive CAS9 expression does not result in any detectable toxicity or morphological abnormalities. To achieve *Rpsa* knockout we injected neonatal (3-5 days post-birth) mice with AAVs encoding for sgRNAs targeting exons 3, 4 and 5 of the *Rpsa* gene, in equal proportions (Figure S2A). The resulting mice are genetic mosaics in which the fraction of cardiomyocytes with *Rpsa* knockout in the heart depends on the transduction efficiency. For controls, we injected mice with an AAV encoding for a non-targeting sgRNA sequence. We confirmed the CRISPR-CAS9-mediated gene editing in the *Rpsa* gene in the mouse heart tissue using a T7 endonuclease I (T7E1) assay (Figure S2B). We first analyzed these unconditional *Rpsa* knockout mice at the age of 3 months. Echocardiography analysis was consistent with dilated cardiomyopathy with increased diastolic and systolic left ventricular dimensions, decreased wall thickness, and reduced systolic function (Figure 4 A-F). Gravimetric analysis supported these findings, showing an elevated heart weight to body weight ratio (Figure 4G).

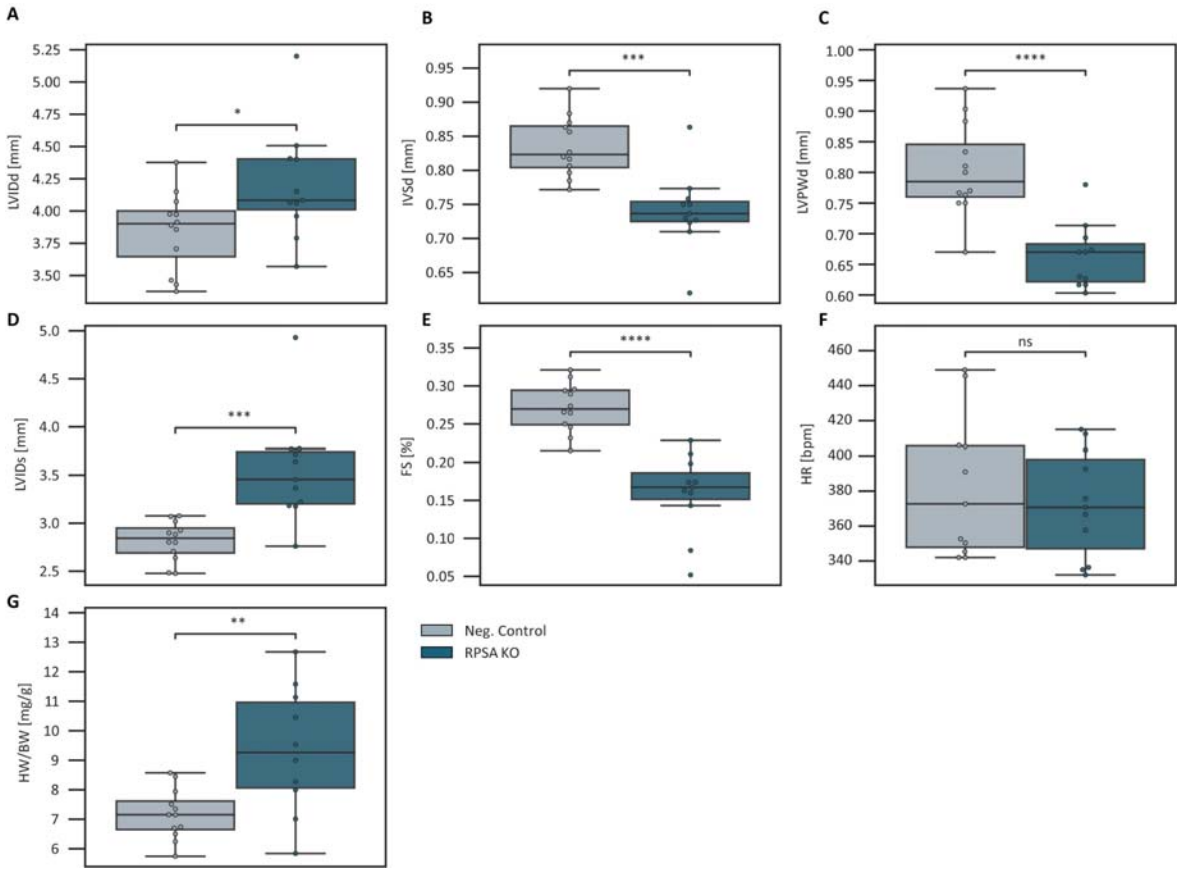

Figure 4. Knockout of RPSA in vivo results in cardiac dysfunction

(A-F) Echocardiographic assessment of mice with unconditional CAS9 expression transduced with AAVs encoding for sgRNAs targeting exons 3, 4 and 5 of *Rpsa* to knockout this gene or control gRNAs. Analysis shows RPSA knockout results in cardiac dilation with increased left ventricular internal diameter at end diastole (LVIDd), wall thinning with decreased interventricular septal and left ventricular posterior wall diameters at end diastole (IVSd and LVPWd), and decreased contractile function with increased left ventricular internal diameter at end systole (LVIDs) and decreased fractional shortening (FS%). Heart rate (HR) was unchanged. N = 11-12 mice per group, mean of 3 measurements per each mouse. p value annotation: ns ($p > 0.05$), * ($p \leq 0.05$), ** ($p \leq 0.01$), *** ($p \leq 0.001$), **** ($p \leq 0.0001$).
(G) Gravimetric analysis showing increased heart weight normalized to body weight **(**HW/BW**)** after RPSA knockout. N = 11-12 mice per group, ** ($p \leq 0.01$).

To ensure that the phenotype resulted from cardiomyocyte cell autonomous loss of *Rpsa* we next used the parental Rosa26-Lox-STOP-lox-Cas9 knockin mouse line. These mice were similarly transduced with AAVs that encode for the sgRNAs targeting *Rpsa* and also express HA-tagged nuclear localized CRE under the control of the chicken cardiac troponin T promoter to delete the STOP cassette and express CAS9, specifically in cardiomyocytes. We also confirmed the CRISPR-CAS9-mediated gene editing in the *Rpsa* gene in the mouse heart tissue using a T7 endonuclease I (T7E1) assay in these mice (Figure S2C). We analyzed mice with cardiomyocytes specific CRE expression at the age of 1, 3, and 6 months. Although the echocardiographic parameters were not significantly changed at the age of 3 months, the same phenotype as in the unconditional *Rpsa* targeted mice manifested at the age of 6 months, with chamber dilation and reduced function (Figure 5 A-F). The delay is likely due to decreased efficiency of the Troponin T driven CRE expressing AAVs compared to the germline β-actin driven CRE. Nevertheless, these data confirm that RPSA knockout induces cardiomyocyte cell-autonomous dilated cardiomyopathy phenotype.

We assessed changes in gene expression using RT-qPCR at the age of 1 and 3 months. Although echocardiography did not show significant changes at the age of 1 month, the fetal genes *Nppa* and *Nppb*, encoding ANP and BNP respectively, and *Myh7* were upregulated, suggesting cardiac stress (Figure 5 G-K). Similarly, markers of the fibrotic reaction *Fn1* and *Col1a1* were upregulated. *Acta1* trended for upregulation and *Myh6* trended for downregulation, but these changes were not statistically significant. At the age of 3 months *Nppa* and *Myh7*

remained elevated, but *Fn1* and *Col1a1* were no longer significantly elevated (Figure 5 L-M). These findings are consistent with dilated cardiomyopathy that started to develop at an early age.

For microscopic analysis we stained cardiac sections from both *Rpsa* knockout and control mice with antibodies targeting ACTN2 and the HA-tag. As the mice are genetic mosaics, only some cardiomyocytes were transduced and showed *Rpsa* knockouts, and we used the HA staining to identify the transduced cardiomyocytes through their HA-CRE nuclear signal. In control mice, HA-positive and HA-negative cells displayed no significant difference in width. However, in *Rpsa* knockout mice, HA-positive cells were significantly smaller in width compared to HA-positive cells in control mice. On the other hand, HA-negative cells in *Rpsa* knockout mice were significantly larger in width compared to HA-negative cells in control mice (Figure 5 N-O). Together these findings show cell atrophy in *Rpsa* knockout cardiomyocytes and a compensatory hypertrophy of the untransduced cardiomyocytes.

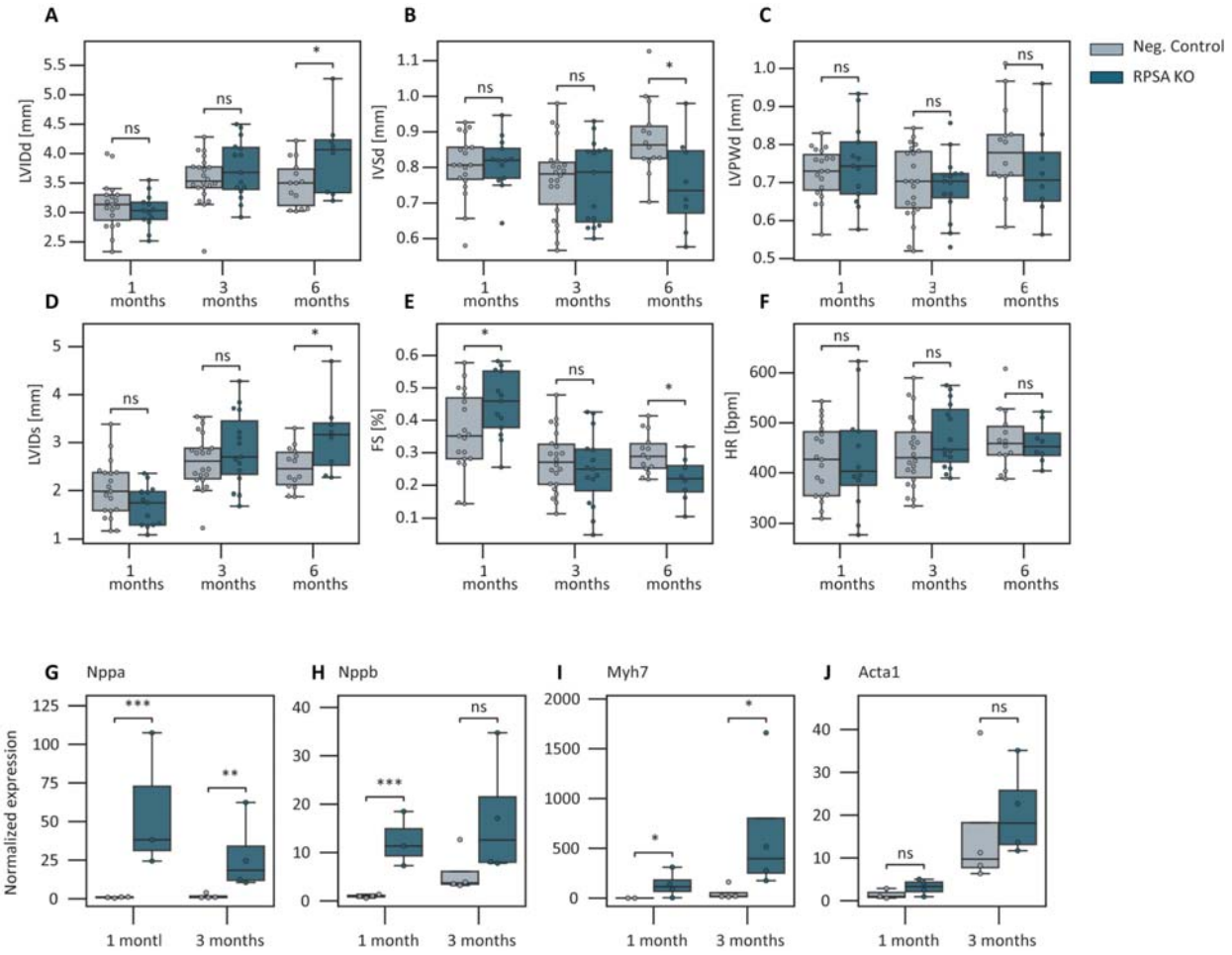

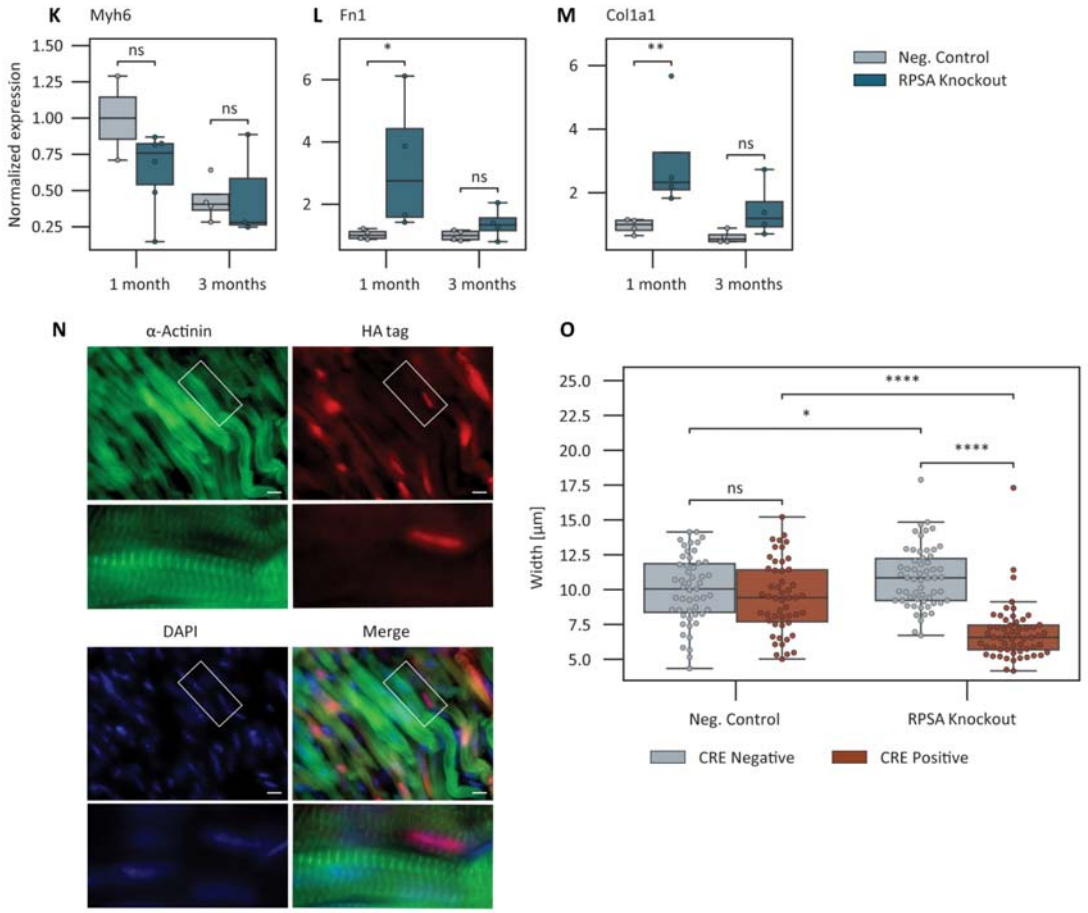

Figure 5. Cardiomyocyte cell autonomous loss of Rpsa results in cardiac dysfunction and cardiomyocyte atrophy.

(A-F) Echocardiographic assessment of mice with Lox-stop-Lox-CAS9 transduced with AAVs encoding for sgRNAs targeting exons 3, 4 and 5 of *Rpsa* or control gRNAs and troponin promoter driven CRE expression to knockout *Rpsa* specifically in cardiomyocytes at 1,3, and 6 months of age. Analysis shows *Rpsa* knockout results in cardiac dilation with increased left ventricular internal diameter at end diastole (LVIDd), wall thinning with decreased interventricular septal and left ventricular posterior wall diameters at end diastole (IVSd and LVPWd), and decreased contractile function with increased left ventricular internal diameter at end systole (LVIDs) and decreased fractional shortening (FS%). Most of these changes are statistically significant only at 6 month of age. Heart rate (HR) was unchanged. N = 17-24 mice per experimental group. mean of 3 measurements per each. p value annotation: ns ($p > 0.05$), * ($p \leq 0.05$), ** ($p \leq 0.01$), *** ($p \leq 0.001$), **** ($p \leq 0.0001$).

(G-M) Gene expression analysis by RT-qPCR shows an increase in markers of cardiac stress

and hypertrophy (*Nppa*, *Nppb*, and *Myh7*) as well as in markers of fibrosis *Fn1* and *Col1a1* in *Rpsa* knockout hearts. Expression data is normalized to *Gapdh*. N = 2-4 mice per age and experimental group. 2-3 technical replicates per mouse. p value annotation: ns ($p > 0.05$), * ($p \leq 0.05$), ** ($p \leq 0.01$), *** ($p \leq 0.001$), **** ($p \leq 0.0001$).

(N-O) Sections from Lox-stop-Lox-CAS9 *Rpsa* knockout and control mosaic mice show decreased cardiomyocytes width in *Rpsa* knockout cardiomyocytes, indicating atrophy, and increased width in non-targeted cardiomyocytes, indicating hypertrophy. Cardiomyocytes identified with α-actinin staining (green) and targeting by the HA-tag staining (red) to identify nuclear HA-CRE. Nuclei stained with DAPI (blue). Representative images from *Rpsa* knockout heart (N), and quantitative analysis in (O). N = 51-58 cells from at least 3 mice per group. p value annotation: ns ($p > 0.05$), * ($p \leq 0.05$), ** ($p \leq 0.01$), *** ($p \leq 0.001$), **** ($p \leq 0.0001$).

Loss of RPSA results in loss of localized translation and loss of ribosome localization in-vivo

Next, we wanted to see if loss of RPSA resulted in the loss of localized protein translation in cardiomyocytes in vivo. We intraperitoneally injected *Rpsa* knockout and control mice with OPP (0.049 mg/g) and after 1 hour, we sacrificed the mice, harvested the hearts, and performed cryosections. The OPP labeling was performed by a Click reaction on the sections and the cells were co-stained for the HA-tag to identify the nuclear HA-CRE in the transduced cells. As we have previously shown[7], the OPP staining displays a characteristic striated pattern, reflecting localized sarcomeric protein translation in wild-type cardiomyocytes. In both control mice cardiomyocytes and in HA-negative cardiomyocytes in the *Rpsa* knockout mice, this striated pattern remained intact, implying normal localized translation at the sarcomeric Z-lines. However, in *Rpsa* knockout mice, HA-positive cells demonstrated a loss of this striation pattern, but not a complete loss of OPP signal, indicating a disruption of localized translation at the sarcomeres but not a complete abrogation of protein translation (Figure 6A-F).

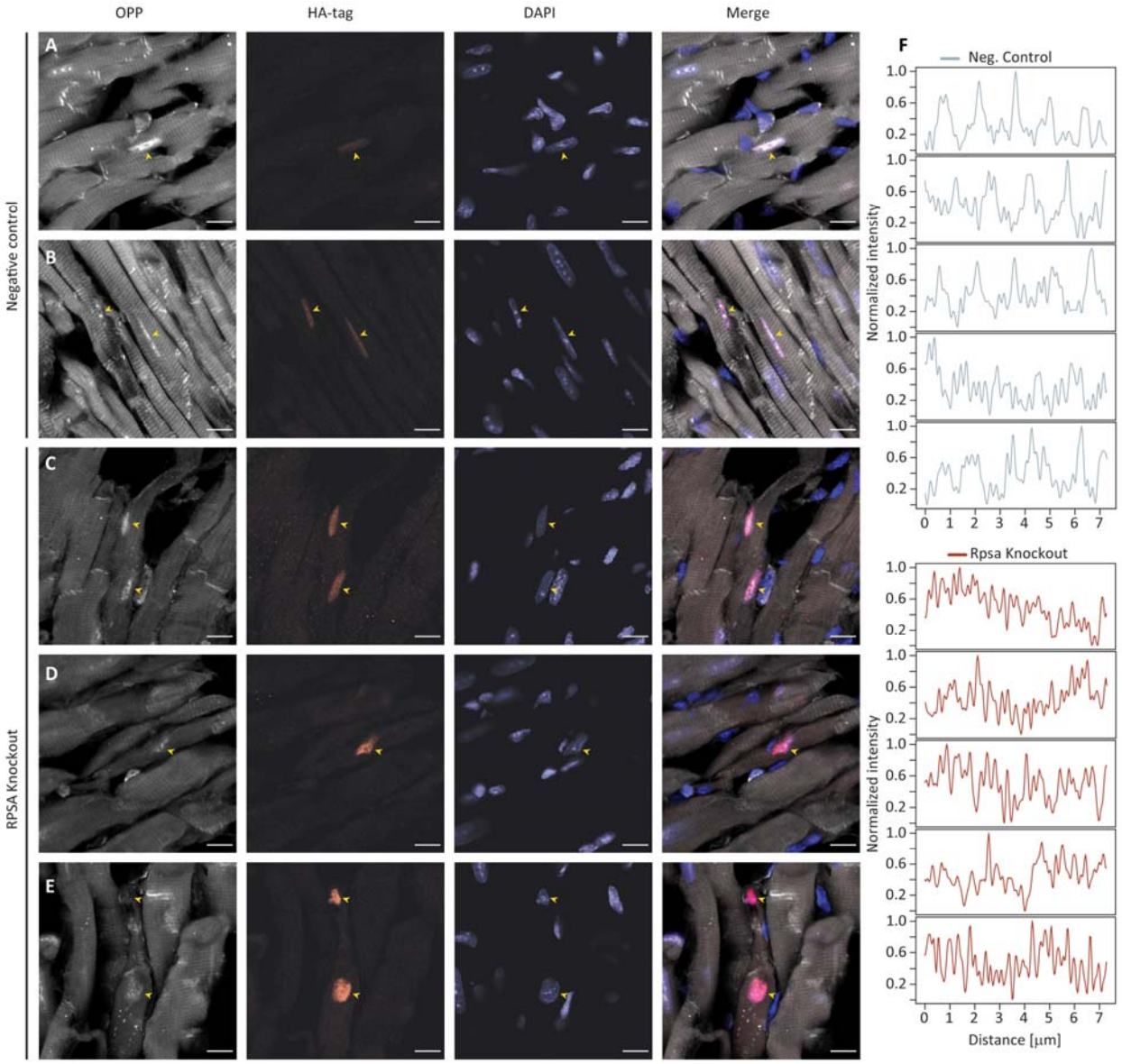

Figure 6. *Rpsa* knockout disrupts local sarcomeric protein translation in-vivo.

(A-E) Mosaic *Rpsa* knockout and control mice were injected with OPP and stained for OPP and HA-CRE to label nascent proteins and identify targeted cardiomyocytes respectively. Representative images show OPP localized sarcomeric cross striated pattern of translation in both targeted and untargeted cardiomyocytes in negative control mice (A-B). In *Rpsa* knockout mice the localized sarcomeric translation is lost in targeted HA-CRE positive cardiomyocytes, while untargeted cells are normal (C-E). OPP-labeled nascent proteins (white), HA-tag (red) and DAPI (blue). Nuclear HA-CRE positive nuclei are labeled with yellow arrowheads. Scale bar = 10 µm.

(F) The intensity of the OPP signal along the cardiomyocytes shows sarcomeric periodicity in targeted cardiomyocytes in negative control mice (grey line). In *Rpsa* knockout mice the sarcomeric periodicity of the localized translation OPP signal is lost in the targeted HA-CRE positive cardiomyocyte (brown line).

We next asked if the loss of localized translation resulted from impaired ribosome localization in *Rpsa* knockout cardiomyocytes. We used dual single-molecule fluorescent in situ hybridization (smFISH) with probes directed at the ribosomal 18S RNA to identify ribosomes and probes targeting the *Cre* mRNA sequence to identify transduced cells. While HA-CRE signal was nuclear due to the nuclear localization signal in CRE proteins, the *Cre* mRNA signal was expected to be predominantly cytoplasmic. In both control and *Rpsa* knockout mice, *Cre*-negative cells maintained a typical striated pattern when probed for 18S rRNA, indicative of normal ribosomal localization (Figure 7A-D). However, in *Rpsa* knockout mice, *Cre*-positive cells exhibited a loss of this striation pattern, showing a disruption in the normal sarcomeric localization of ribosomes. RPSA loss disrupted ribosome localization but did not eliminate ribosomes, explaining why localized translation was lost in the OPP assay but protein translation was not completely abrogated.

The N-terminal domain (amino acids 1–209) of RPSA is globular highly conserved region which shares high resemblance to the prokaryotic ribosomal proteins S2 (RPS2) family.[10] This region was shown to be sufficient for ribosomal binding. The C-terminal domain (amino acids 210-295) is absent in prokaryotes and has an intrinsically disordered structure. We therefore wanted to verify if the C-terminal domain of RPSA was sufficient for localization to the sarcomere. We expressed HA-tagged-mCherry-RPSA-C-Terminal fragment$_{210\text{-}295}$ in mice using AAVs. A staining of cardiac sections from these mice with anti-HA and anti-ACTN2 antibodies showed the C-terminus of RPSA was sufficient to localize the construct at the same location as endogenous RPSA and ribosomes, on both sides of the Z-line (Fig. S3).

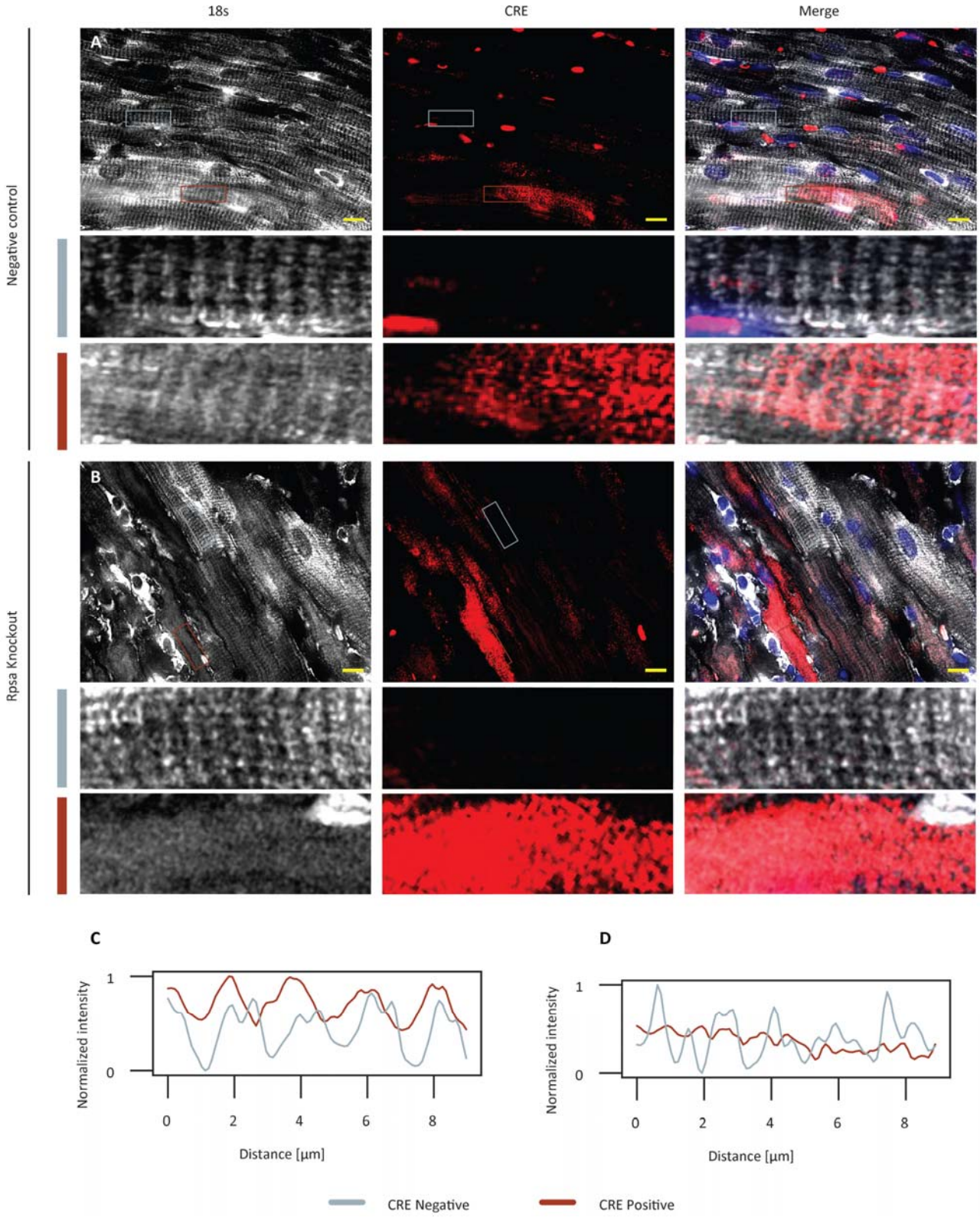
18s
CRE
Merge
A
B
Negative control
Rpsa Knockout
C
D
Normalized intensity
1
0
0
2
4
6
8
Distance [µm]
CRE Negative
CRE Positive

Figure 7. *Rpsa* knockout disrupts sarcomeric ribosome localization in-vivo.
(A-B) Dual smFISH with probes for ribosomal18S RNA (white) and *Cre* mRNA (red) was used to visualize ribosomes and targeted cardiomyocytes respectively. Representative images show sarcomeric cross striated pattern of ribosomes localization in both targeted and untargeted cardiomyocytes in negative control mice (A). In *Rpsa* knockout mice the sarcomeric localization of ribosomes is lost in targeted *Cre* positive cardiomyocytes, while untargeted cells are normal (B). Inset shows magnification of untargeted cytoplasmic *Cre* mRNA negative cell (grey rectangle) and targeted cytoplasmic *Cre* mRNA positive cell (brown rectangle) for both the negative control (A) and *Rpsa* knockout (B) hearts. Scale bar = 10 µm.
(C-D) The intensity of ribosomal 18S RNA FISH signal along the cardiomyocytes in the inset shows sarcomeric periodicity in both the targeted (brown line) and untargeted (grey line) cardiomyocytes in negative control mice (C). In *Rpsa* knockout mice (D) the sarcomeric periodicity of ribosomes is lost in the targeted *Cre* positive cardiomyocyte (brown line), while the untargeted cell has normal periodicity (grey line).

Discussion

Here we used proximity ligation to unravel the Z-line proteome and identified RPSA as a potential localization candidate. We show that RPSA is required for localization of ribosomes, for the localization of translation, and for sarcomere maintenance in cardiomyocytes in vivo. The loss of RPSA causes the ribosomes and translation to lose their sarcomeric localization, eventually leading to dilated cardiomyopathy. In genetic mosaic mice the untraduced cells undergo compensatory hypertrophy in response to the atrophy of the RPSA knockout cardiomyocytes. RPSA is known to bind the microtubular system[12], and we also show here that the C-terminus extra-ribosomal domain of RPSA is sufficient for localization to the Z-line of the sarcomere.

We used Cypher (LDB3) as our bait for the spatial proteomic analysis. This protein interacts through its N-terminal PDZ domain with the Z-line protein α-actinin[13], and BioID2 was tethered to its C-terminal part. We showed that the bait is localized to the Z-line, and our proteomic analysis identified multiple know Z-line proteins including α-actinin, other PDZ-Lim proteins such as Enigma (Pdlim7) and Enigma Homologue (Pdlim5), Palladin, and Myozenin, confirming that we specifically enriched for Z-line proteins. We also identified multiple proteins associated with ribosomes and protein translation, providing further evidence that this region is an important

protein translation hub. A previous study used proximity labeling experiment to unravel the Z-line proteome.[14] As compared with our study, this study used human iPS-derived cardiomyocytes, which are less structurally mature than neonatal rat cardiomyocytes, a different bait, α-actinin instead of Cypher, and a different control – no BioID as opposed to untethered BioID here. While several ribosomal proteins were identified in this study, RPSA was not among the significant hits, and interestingly IGF2BP2, a major hit, was not identified in our study. The width of the Z-line measured by electron microscopy is 130 nm.[15] and the exact location of the C-terminus of Cypher within the structure is not known. Given the uncertainty regarding the exact localization of Cypher C-terminus and that BioID has a practical labeling radius estimated at ~10 nm[16], it is difficult to determine precisely where the ribosomal and translation nanodomain resides inside or near the Z-line. Our co-immunostaining of RPSA and α-actinin suggests that ribosomes or at least RPSA mostly reside on both sides of the Z-line at the lateral ends of the I-band. We speculate therefore that we mostly isolated proteins from a nanodomain located on both sides of the of the Z-line while the α-actinin-BioID study identified a domain that is more at the center of the of the Z-line.

There is controversy over the location and functions of RPSA. RPSA was separately identified as a non-integrin laminin receptor with a 67-kDa molecular weight from muscle cell membranes[17] and as a component of the 40S ribosome with a 32-37- kDa molecular weight[18] and was called 37/67-kDa laminin receptor (LAMR). It was reported to reside in the plasma membrane, the ribosomes, the cytosol, and the nucleus.[10] There are many unanswered questions regarding the cellular biology of this protein, about its ability to bind laminin, and about the function of its intrinsically disordered C-terminal region.[10] While RPSA's N-terminal domain (amino acids 1-209) is homologous to the bacterial small ribosomal protein rps2, its C-terminal domain (amino acids 210-295) is not found in prokaryotes. It was therefore proposed that the N-terminal domain binds ribosomes while the C-terminal domain of RPSA functions in laminin binding. Nevertheless, it was also proposed that the C-terminal domain of RPSA participates in ribosome binding.[19]

It is also unclear how RPSA functions as a ribosomal protein. It is highly abundant, with six to eight copies per ribosome, and does not appear to be a constitutive component of ribosomes.[19–21] We found that in cardiomyocytes RPSA is localized to both sides of the Z-line and near the intercalated discs. This location coincides with our previously documented location of ribosomes[7,8], and together with the proteomic analysis here, that identified other ribosomal protein at this site, suggests that RPSA is predominantly associated with ribosomes near the Z-

lines of cardiomyocytes. We showed that the sarcomeric localization of ribosomes was lost after deletion of RPSA in vivo. In cardiomyocytes and muscle cells, the bulk of the transcriptome is located along the Z-line[7,8], including transcripts for non-sarcomeric prtoeins.[9] We and others have also shown that this mRNA distribution does not depend on ribosomes and translation.[7,9] The untethering of ribosomes from the Z-line should increase the distance between ribosomes and mRNAs, resulting in a decrease in protein translation. Indeed, we show that localized translation in cardiomyocytes, was lost after knockdown of RPSA in cultured cardiomyocytes or by CRISPR knockout in vivo.

Although knockout of RPSA resulted in cardiomyocyte atrophy, we could identify knockout cardiomyocytes even several months after RPSA ablation and could show these cardiomyocytes contained ribosomes and exhibited translation, albeit reduced and unlocalized. Considering the limited half-lives of proteins in the heart[22], these results strongly suggest that RPSA is not required for ribosome biogenesis or protein translation in general. However, we cannot rule out that RPSA has additional ribosomal functions in addition to localization. This question is further complicated by the fact that ribosomes are responsible for the translation of ribosomal proteins, and therefore the untethering of ribosomes from the Z-lines and from the localized mRNAs there is also expected to reduce the translation of ribosomal proteins, leading to further reduction in translation.

Proteomic pull-down in fibroblast showed that RPSA interacts with cytoskeletal elements in addition to its interactions with multiple ribosomal proteins.[23] In particular, elements of the microtubular system including tubulin and Dynein cytoplasmic 1 intermediate chain 2, a molecular motor protein responsible for transport of proteins along microtubules were identified. A biochemical study showed that recombinant RPSA, but not the bacterial orthologue rps2, directly bind both tubulin and actin with high affinity, suggesting that the C-terminal domain of RPSA, that is absent in bacteria, mediates this interaction.[12] This study also suggested that ablation of the microtubular system results in altered distribution of ribosomes in cultured fibroblasts. We have previously shown that the sarcomeric Z-line association of ribosomes and translation is lost upon ablation of the microtubular system.[7,8] Together with our observation that the C-terminal domain of RPSA is sufficient for binding to the Z-line these data imply that RPSA ability to bind to the microtubular system by its C-terminal domain and its ability to bind ribosomes is responsible for ribosomal Z-line localization of ribosomes and translation in cardiomyocytes. We cannot rule out however that the localization is mediated by binding of RPSA to additional proteins.

A spontaneously occurring mutation in *Rpsa* in a mouse line resulted in arrhythmogenic right ventricular cardiomyopathy, that was ascribed to nuclear functions of RPSA and binding to heterochromatin protein 1, suggesting that this gene may have a specific function in the heart.[24] However, homozygous *Rpsa* knockout mice die at an early embryonic age, and therefore the necessity for this gene could not be studied in vivo.[10] In this study, we used a cardiomyocyte-specific genetic mosaic knockout of *Rpsa* to investigate the cardiomyocyte cell-autonomous effects of RPSA loss in post-natal cells within the context of normally functioning myocardium, although the mice eventually succumbed to cardiomyopathy. A knockout of *Rpsa* in all cardiomyocytes would have likely resulted in profound cardiac dysfunction and would have made the dissection of the direct effects of RPSA deletion the from secondary effects difficult.[25]

The role of RPSA in tethering ribosomes to microtubules has been proposed before[12], but the highly localized and cross striated distribution of ribosomes and translation in cardiomyocytes allowed us to examine and demonstrate the necessity of RPSA for localized translation in vivo. It is likely however that RPSA is required for localized translation in many cell types. Multiple mechanisms were shown to be responsible for mRNA localization in different cell types and cellular locations[26], and therefore it is possible, or even likely, that additional mechanisms and elements are responsible for ribosome and translation localization beyond RPSA in muscle cell and in additional cell types.

Methods

sgRNAs

Species	**Target**	**Top strand (5'-3')**	**Bottom strand (5'-3')**
Mus musculus	None	ACCGGCGAGGTATTCGGCTCCGCG	AAACCGCGGAGCCGAATACCTCGC
Mus musculus	Rpsa	ACCGGGTTTATGATGTAGATACCT	AAACAGGTATCTACATCATAAACC
Mus musculus	Rpsa	ACCGCAAGTACCTTGTTGTTGCAT	AAACATGCAACAACAAGGTACTTG
Mus musculus	Rpsa	CTTACAGGGAGCTCACTCAG	CTGAGTGAGCTCCCTGTAAG

Antibodies

Name	Manufacturer	Catalog #
Anti-Cardiac Troponin I antibody	Abcam	ab47003
Anti-alpha-Actinin antibody	Sigma-Aldrich	A7811
Anti-BioID2 antibody [SS 3A5-E2]	Abcam	ab232733
Anti-67kDa Laminin Receptor antibody [EPR8469]	Abcam	ab133645
Anti HA-tag antibody	Abcam	ab9110

Plasmids

pAAV2/9n (Addgene plasmid #112865; http://n2t.net/addgene:112865; RRID: Addgene_112865) and pAdDeltaF6 (Addgene plasmid #112867; http://n2t.net/addgene:112867; RRID: Addgene_112867) were a gift from James M. Wilson. mycBioID2-pBABE-puro was a gift from Kyle Roux (Addgene plasmid #80900; http://n2t.net/addgene:80900; RRID: Addgene_80900).

Isolation of cardiomyocytes and tissue culture

NRVMs were isolated using the Worthington Biochemical Neonatal Cardiomyocyte Isolation system (Cat. #LK003300) according to the manufacturer's instructions. The cells were loaded onto a 5 ml Percoll gradient composed of high concentration (60% Percoll) and low concentration (35% Percoll) in ADS buffer. This was then centrifuged for 30 min at 1730g with slow deceleration using a tilting bucket rotor. This allowed for the separation of cardiomyocytes using gentle aspiration of the appropriate band. The isolated cardiomyocytes were resuspended in a growing medium consisting of DMEM:F-12 supplemented with 15% fetal bovine serum, penicillin-streptomycin, and L-glutamine. Cytosine β-D-arabinofuranoside (ARA-C, Sigma-Aldrich #C1768) was added to the culture medium for a final concentration of 3 µM to inhibit the proliferation of fibroblasts. The cells were then seeded and incubated for 24 hours to allow for attachment.

ADS buffer: Sodium Chloride (NaCl) [116.4 mM], Potassium Chloride (KCl) [5.4 mM], Dextrose [5.6 mM], Monosodium Phosphate (NaH2PO4 * H2O) [10.9 mM], Magnesium Phosphate (MgSO4) [0.4057 mM], and HEPES [20 mM].

Isolation of adult rat ventricular cardiomyocytes was performed according to the previously published protocol.[27] Briefly, an adult rat was anesthetized using a combination of ketamine and xylazine. The heart was excised and placed in ice-cold Krebs-Henseleit buffer containing 1 mM Ca^{2+} (KHB-Ca^{2+}). The aorta was then cannulated, and the heart was attached to a perfusion

apparatus. Retrograde perfusion started with a KHB for 5 minutes. Next, the solution was replaced with KHB containing 162 U/mL Type II Collagenase (Worthington) and perfusion resumed for an additional 15 minutes. $CaCl_2$ was gradually added to the reperfusion solution over 15 minutes to achieve a final concentration of 0.75 mM. The heart was then removed and minced in KHB-Ca^{2+} containing Collagenase. Gentle trituration was performed, and the mixture was centrifuged. The cardiomyocytes-enriched pellet was resuspended in KHB containing 2% BSA and 1 mM $CaCl_2$. $CaCl_2$ was gradually added over 15 minutes to achieve a final concentration of 1.75 mM.

The mixture was then centrifuged again and cardiomyocytes were resuspended in DMEM containing 5% fetal bovine serum.

Production of adenoviruses

HEK293 cells were transfected with an adenovirus expression plasmid containing the insert (Chypher-BioID2 or BioID2). Cells were then incubated for 1-2 weeks and observed daily. Once 50% of the cells exhibited cytopathic effects, they were collected. Lysis was performed by subjecting the cells to 3 cycles of freezing and thawing. Cell debris was removed from the sample using centrifugation and the supernatant was used to transduce a larger amount of HEK293. This amplification process was repeated to produce the desired titer.

Production of adeno-associated Viruses

The production of AAV followed a previously published protocol[28]. Briefly, desired inserts were cloned into a pAAV plasmid. HEK293 cells were transfected with the pAAV plasmid, along with a helper plasmid (pAdDeltaF6) and a packaging plasmid (pAAV2/9n). Transfection was performed using pH-titrated linear Polyethyleneimine (PEI). Three days following transfection, the medium was removed and stored at 4ºC, and fresh medium was added. Following an additional two days, the medium was again removed and stored, and the cells were harvested. The cells were then resuspended with nuclease, and a solution of Polyethylene Glycol (PEG) 40% (Sigma Aldrich) at one-fifth the volume was added. The mixture was centrifuged at 4ºC for 30 minutes at 4,000g, and the resulting pellet was resuspended in nuclease. The two solutions were combined, loaded onto an Iodixanol gradient, and subjected to ultracentrifugation at 200,000g for 2.5 hours at 18ºC using a tilting bucket rotor. The band containing the virus appeared at the 40%/60% interphase of the gradient and was aspirated using a syringe. Buffer exchange was performed using an Amicon Ultra 15ml 100K (Millipore, UFC9100) to DPBS. Virus titration was conducted by qRT-PCR using plasmid serial dilutions as a standard for calibration purposes.

For injection of AAV to mice, 50 µL of containing approximately $3*10^{11}$ viral genomes were injected into the intraperitoneal cavity of 3-5 days old mouse pups.

Microscopy

Samples were imaged using either a confocal or a widefield microscope. For confocal imaging, samples were imaged using a Zeiss LSM 900 with Airyscan2 super-resolution system, attached to an Axio Observer 7 inverted microscope. Acquisition was performed with Plan-Apochromat 63x/1.4 oil DIC M27 objective from Zeiss. Airyscan images were processed with the ZEN software using default parameters.

For widefield imaging, slides were imaged with Axio Observer inverted fluorescent microscope (Zeiss) using an X-cite metal-halide light source and a high-resolution camera (Hamamatsu Orca R2), with an X63/1.4NA objective (Olympus).

Image analysis

For automated image analysis of OPP and immunofluorescence signals a custom tool based on the Sarcomere Texture Analysis (SOTA) method[29] was developed. Briefly, cells were segmented from multi-channel immunofluorescence images and algorithms were used to quantify two aspects of the sarcomeric structure, namely homogeneity and co-localization of different markers.

Immunofluorescence staining

Immunofluorescence staining was performed on isolated cardiomyocytes and frozen heart tissue sections. For immunofluorescence combined with OPP assay, immunostaining was performed first, followed by the OPP assay as described below. Cells and tissue were permeabilized with 1% Triton or 70% ethanol and blocked with a solution containing 5% fetal bovine serum. Primary antibodies were incubated overnight at 4 °C. Secondary antibodies were incubated for 1 hour at room temperature. Nuclei were counterstained with DAPI for 10 min at room temperature.

Rodents

All in vivo experiments were performed according to the Technion IACUC guidelines. All procedures and protocols were approved in advance. Mice and rats were maintained in a Specific Pathogen Free facility, with temperature and humidity control and a 12-hour light cycle. Techniplast cages were used, with ad libitum water and food supply. Male and females were equally used.

Tissue sections

The hearts were removed, cut in half, and flushed with ice-cold PBS. Fixation was performed by incubating the tissue fragments in 3.5% formaldehyde in PBS. Following fixation, samples were incubated overnight at 4°c in a cryoprotective solution (30% sucrose, 3.5% formaldehyde in PBS). The following day, samples were flushed with ice-cold PBS, placed in OCT compound embedding matrix (Tissue-Tek #4583) and snap-frozen in 2-methylbutane immersed in liquid nitrogen. Sectioning was performed using a cryostat (Leica). Individual sections were mounted on silane-coated glass slides.

Single-molecule FISH

For each target, a set of Stellaris RNA FISH probes (Biosearch technologies) was designed. These sets comprised of up to 48 single-labeled, 18-22 nucleotides long oligos designed to selectively bind to the target transcript. Probes were tagged with either 5-TAMRA or Quasar-670 fluorophores. smFISH was performed according to the manufacturer's protocol. Briefly, samples were fixed using 3.7% Formaldehyde in 1x PBS, incubated for 10 minutes at room temperature, washed twice in 1x PBS, and incubated in 70% ethanol for a minimum of 1 hour at 4°c to facilitate permeabilization. Following this incubation, the samples were washed in a wash buffer (10% formamide in 2x SSC) and placed in a humidified chamber. The probe of choice was then added to the hybridization buffer (100 mg/mL dextran sulfate, 10% formamide in 2x SSC) for a final concentration of 125 nM. This mixture was then applied to the samples and the samples were incubated at 37°c overnight. The next day, samples were washed with a wash buffer, DAPI was applied, and the samples washed again. Prior to mounting, samples were incubated in 2X SSC for 2-5 minutes. Mounting was performed using GLOX anti-fade buffer and the samples were imaged immediately.

Slides were imaged with Axio Observer inverted fluorescent microscope (Zeiss, see under microscopy). Exposure times for smFISH signals were between 800-3000 milliseconds. Images were acquired as a full thickness z-stack with a 0.24 µm section thickness. For qualitative analysis, images were imported into the ImageJ software, a Laplacian of Gaussian filter was applied to the smFISH channels using the Log3D plugin, and a maximum intensity merge of the z-stack was performed.

RT-qPCR

For cell cultures, RNA was isolated using the NucleoSpin RNA (Macherey-Nagel #740955) according to the manufacturer's instructions. For isolation of RNA from heart tissues, a Bullet Blender homogenizer (Next Advance) was used to homogenize the tissue prior to the standard

protocol of RNA extraction. Following RNA isolation, cDNA was produced by reverse transcription. qRT-PCR was performed using a Bio-Rad CFX96 thermocycler. All studies were performed with a standard curve, technical duplicates or triplicates, and controls (negative control and no reverse transcriptase control).

BioID Proximity Labeling Assay

NRVM were transduced using adenoviruses encoding either 3x-HA-Cypher1s-mycBioID2 (bait construct) or mycBioID2 (control construct). Cells were then incubated for 48 hours to allow for expression of the encoded constructs. Culture medium was replaced by NRVM medium supplemented with 50 µM Biotin and the cells were incubated for 18 hours to allow for labelling. Subsequently, culture plates were placed on ice, culture medium was aspirated, and plates were thoroughly washed with ice-cold PBS. Cells were then scraped in 1 mL of PBS and centrifuged. The cell pellet was then frozen in liquid nitrogen and stored at -80°c until pull-down.

Pull-down

Pull-down procedure was based on a previously published protocol[30]. Briefly, cell pellets were resuspended in lysis buffer (50 mM Tris-HCl, 500 mM NaCl, 0.2% SDS, 1 mM DTT and 1x protease inhibitors cocktail) and pooled. Triton X-100 was added to the suspended pellets and the samples were then vortexed and placed on ice for all subsequent steps. Samples were then sonicated twice [1 minute each, 6/14 cycle, 30% output level]. Tris-HCl was added to the samples and a third sonication was performed using the same settings. Samples were then centrifuged, and the supernatant was transferred to a tube containing Streptavidin magnetic beads (EMD Millipore). Samples were then incubated overnight at 4°c with constant rotation.

The following day, samples were placed on a magnetic stand and beads were allowed to settle. Beads were washed two times with wash buffer 1 (2% SDS), once with wash buffer 2 (0.1% Deoxycholic acid, 1% Triton X-100, 1 mM EDTA, 500 mM NaCl, 50 mM HEPES), once with wash buffer 3 (250 mM Lithium chloride, 10 mM Tris-HCl, 1 mM EDTA, 0.5% NP-40, 0.5% Deoxycholic acid) and three times with 50 mM Tris-HCl. Following the last wash, supernatant was removed, beads were resuspended in 50 mM Ammonium Bicarbonate and stored at -80°c.

Mass spectrometry

Samples were digested on beads using trypsin and analyzed by LC-MS/MS on Q Exactive Plus (Thermo-fisher)

Analysis

Proteomic analysis was performed using MaxQuant and Perseus with log2 of LFQ values. Proteins that have been identified by less than two distinct peptides were removed. In addition, a protein was considered for the dataset and for further analysis if it had a valid value in two or more replicates in at least one of the groups (control or experiment). Imputation of missing values was performed using Perseus by random numbers drawn from a normal distribution. We used a cutoff of log2FC≥1 and t test $p<0.05$ for significantly enriched proteins. The R EnhancedVolcano package (Blighe, K, S Rana, and M Lewis. 2018. "EnhancedVolcano: Publication-ready volcano plots with enhanced colouring and labeling.") was used to draw volcano plots. The ShinyGO 0.77 tool was used for pathway enrichment.[31] STRING was used for visualization.[32]

OPP assay

Analysis of the location of protein synthesis was performed using the Click-iT Plus OPP Alexa Fluor 488 Protein Synthesis Assay Kit (Thermo-Fischer Scientific). Briefly, cells were incubated with o-propargyl-puromycin (OPP) to facilitate labeling of nascent proteins. Following incubation, cells were washed thoroughly, fixed with 4% formaldehyde in 1x PBS and permeabilized using 0.5% triton. A copper-catalyzed azide-alkyne cycloaddition reaction (click reaction) was performed between the alkyne-containing OPP and the azide-conjugated fluorophore.

For in-vivo protein synthesis assay mice were injected intraperitoneally with OPP (0.049 mg/gr). Mice were sacrificed one hour following OPP injection. The heart was then removed frozen and cryosectioned.

Statistics

Data is shown as mean ± SD or SE as indicated. A two tailed student's t-test was used for comparison unless stated otherwise.

Funding

Funding for this work was provided by the Israel Science Foundation (grant # 1385/20) and by the Foundation Leducq Research grant no. 20CVD01 to IK

Acknowledgements

The authors wish to thank the Biomedical Core Facility at the Faculty of Medicine, Technion; the Pre – Clinical Research Authority at the Technion, and the Smoler Proteomics Center, Technion-Israel Institute of Technology

References

1. Bourke AM, Schwarz A, Schuman EM. De-centralizing the Central Dogma: mRNA translation in space and time. *Molecular Cell*.

2. Das S, Vera M, Gandin V, Singer RH, Tutucci E. Intracellular mRNA transport and localized translation. *Nature Reviews Molecular Cell Biology*.

3. Martin TG, Kirk JA. Under construction: The dynamic assembly, maintenance, and degradation of the cardiac sarcomere. *Journal of Molecular and Cellular Cardiology*.

4. Hamdani N, Borbély A, Veenstra SPGR, Kooij V, Vrydag W, Zaremba R, Remedios C Dos, Niessen HWM, Michel MC, Paulus WJ, Stienen GJM, Velden J Van Der. More severe cellular phenotype in human idiopathic dilated cardiomyopathy compared to ischemic heart disease. *J Muscle Res Cell Motil* 2010;**31**:289–301.

5. Witjas-Paalberends ER, Piroddi N, Stam K, Dijk SJ van, Oliviera VS, Ferrara C, Scellini B, Hazebroek M, Cate FJ ten, Slegtenhorst M van, Remedios C dos, Niessen HWM, Tesi C, Stienen GJM, Heymans S, Michels M, Poggesi C, Velden J van der. Mutations in MYH7 reduce the force generating capacity of sarcomeres in human familial hypertrophic cardiomyopathy. *Cardiovasc Res* 2013;**99**:432–441.

6. Chen CY, Caporizzo MA, Bedi K, Vite A, Bogush AI, Robison P, Heffler JG, Salomon AK, Kelly NA, Babu A, Morley MP, Margulies KB, Prosser BL. Suppression of detyrosinated microtubules improves cardiomyocyte function in human heart failure. *Nat Med* 2018;**24**:1225–1233.

7. Lewis YE, Moskovitz A, Mutlak M, Heineke J, Caspi LH, Kehat I. Localization of transcripts, translation, and degradation for spatiotemporal sarcomere maintenance. *J Mol Cell Cardiol* 2018;**116**:16–28.

8. Scarborough EA, Uchida K, Vogel M, Erlitzki N, Iyer M, Phyo SA, Bogush A, Kehat I, Prosser BL. Microtubules orchestrate local translation to enable cardiac growth. *Nat Commun* 2021;**12**.

9. Denes LT, Kelley CP, Wang ET. Microtubule-based transport is essential to distribute RNA and nascent protein in skeletal muscle. *Nature Communications 2021 12:1* 2021;**12**:1–19.

10. Digiacomo V, Meruelo D. Looking into laminin receptor: Critical discussion regarding the non-integrin 37/67-kDa laminin receptor/RPSA protein. *Biological Reviews* 2016;**91**:288–310.

11. Sutcliffe MD, Tan PM, Fernandez-Perez A, Nam YJ, Munshi N V., Saucerman JJ. High content analysis identifies unique morphological features of reprogrammed cardiomyocytes. *Sci Rep* 2018;**8**.

12. Venticinque L, Jamieson K V., Meruelo D. Interactions between laminin receptor and the cytoskeleton during translation and cell motility. *PLoS One* 2011;**6**.

13. Klaavuniemi T, Ylänne J. Zasp/Cypher internal ZM-motif containing fragments are sufficient to co-localize with α-actinin-Analysis of patient mutations. *Exp Cell Res* 2006;**312**:1299–1311.

14. Ladha FA, Thakar K, Pettinato AM, Legere N, Ghahremani S, Cohn R, Romano R, Meredith E, Chen YS, Hinson JT. Actinin BioID reveals sarcomere crosstalk with oxidative metabolism through interactions with IGF2BP2. *Cell Rep* 2021;**36**:109512.

15. Burgoyne T, Morris EP, Luther PK. Three-Dimensional Structure of Vertebrate Muscle Z-Band: The Small-Square Lattice Z-Band in Rat Cardiac Muscle. *J Mol Biol* 2015;**427**:3527–3537.

16. Kim DI, Birendra KC, Zhu W, Motamedchaboki K, Doye V, Roux KJ. Probing nuclear pore complex architecture with proximity-dependent biotinylation. *Proc Natl Acad Sci U S A* 2014;**111**.

17. Lesot H, Kühl U, Mark K von der. Isolation of a laminin-binding protein from muscle cell membranes. *EMBO J* 1983;**2**:861–865.

18. Tohgo A, Takasawa S, Munakata H, Yonekura H, Hayashi N, Okamoto H. Structural determination and characterization of a 40 kDa protein isolated from rat 40 S ribosomal subunit. *FEBS Lett* 1994;**340**:133–138.

19. Malygin AA, Babaylova ES, Loktev VB, Karpova GG. A region in the C-terminal domain of ribosomal protein SA required for binding of SA to the human 40S ribosomal subunit. *Biochimie* 2011;**93**:612–617.

20. García-Hernández M, Davies E, Baskin TI, Staswick PE. Association of Plant p40 Protein with Ribosomes Is Enhanced When Polyribosomes Form during Periods of Active Tissue Growth. *Plant Physiol* 1996;**111**:559–568.

21. Auth D, Brawerman G. A 33-kDa polypeptide with homology to the laminin receptor: component of translation machinery. *Proceedings of the National Academy of Sciences* 1992;**89**:4368–4372.

22. Lau E, Cao Q, Ng DCM, Bleakley BJ, Dincer TU, Bot BM, Wang D, Liem DA, Lam MPY, Ge J, Ping P. A large dataset of protein dynamics in the mammalian heart proteome. *Sci Data* 2016;**3**:160015.

23. Venticinque L, Meruelo D. Comprehensive proteomic analysis of nonintegrin laminin receptor interacting proteins. *J Proteome Res* 2012;**11**:4863–4872.

24. Asano Y, Takashima S, Asakura M, Shintani Y, Liao Y, Minamino T, Asanuma H, Sanada S, Kim J, Ogai A, Fukushima T, Oikawa Y, Okazaki Y, Kaneda Y, Sato M, Miyazaki JI, Kitamura S, Tomoike H, Kitakaze M, Hori M. Lamr1 functional retroposon causes right ventricular dysplasia in mice. *Nat Genet* 2004;**36**:123–130.

25. Guo Y, Vandusen NJ, Zhang L, Gu W, Sethi I, Guatimosim S, Ma Q, Jardin BD, Ai Y, Zhang D, Chen B, Guo A, Yuan GC, Song LS, Pu WT. Analysis of Cardiac Myocyte Maturation Using CASAAV, a Platform for Rapid Dissection of Cardiac Myocyte Gene Function in Vivo. *Circ Res* 2017;**120**:1874–1888.

26. Mofatteh M, Bullock SL. SnapShot: Subcellular mRNA Localization. *Cell* 2017;**169**:178-178.e1.

27. Michele DE, Albayya PP, Metzger JM. Thin filament protein dynamics in fully differentiated adult cardiac myocytes: Toward a model of sarcomere maintenance. *Journal of Cell Biology* 1999;**145**:1483–1495.

28. Challis RC, Kumar SR, Chan KY, Challis C, Jang MJ, Rajendran PS, Tompkins JD, Shivkumar K, Deverman BE, Gradinaru V. Widespread and targeted gene expression by systemic AAV vectors: Production, purification, and administration. *bioRxiv* 2018:246405.

29. Sutcliffe MD, Tan PM, Fernandez-Perez A, Nam YJ, Munshi N V., Saucerman JJ. High content analysis identifies unique morphological features of reprogrammed cardiomyocytes. *Scientific Reports 2018 8:1* 2018;**8**:1–11.

30. Cho KF, Branon TC, Udeshi ND, Myers SA, Carr SA, Ting AY. Proximity labeling in mammalian cells with TurboID and split-TurboID. *Nature Protocols 2020 15:12* 2020;**15**:3971–3999.

31. Ge SX, Jung D, Jung D, Yao R. ShinyGO: a graphical gene-set enrichment tool for animals and plants. *Bioinformatics* 2020;**36**:2628–2629.

32. Szklarczyk D, Kirsch R, Koutrouli M, Nastou K, Mehryary F, Hachilif R, Gable AL, Fang T, Doncheva NT, Pyysalo S, Bork P, Jensen LJ, von Mering C. The STRING database in 2023: protein–protein association networks and functional enrichment analyses for any sequenced genome of interest. *Nucleic Acids Res* 2023;**51**:D638–D646.

Figure legends Supplement

Table 1. Identified protein by Cypher-BioID2 and BioID2 triplicates. The LFQ values for each sample are shown with the Log2 of the fold change and the t-test p value.